NJC

Accepted Manuscript

This is an *Accepted Manuscript*, which has been through the Royal Society of Chemistry peer review process and has been accepted for publication.

Accepted Manuscripts are published online shortly after acceptance, before technical editing, formatting and proof reading. Using this free service, authors can make their results available to the community, in citable form, before we publish the edited article. We will replace this *Accepted Manuscript* with the edited and formatted *Advance Article* as soon as it is available.

You can find more information about *Accepted Manuscripts* in the Information for Authors.

Please note that technical editing may introduce minor changes to the text and/or graphics, which may alter content. The journal's standard Terms & Conditions and the Ethical guidelines still apply. In no event shall the Royal Society of Chemistry be held responsible for any errors or omissions in this *Accepted Manuscript* or any consequences arising from the use of any information it contains.

ROYAL SOCIETY OF CHEMISTRY

www.rsc.org/njc

New Journal of Chemistry

RSCPublishing

ARTICLE

Self-assembly of ultrathin mesoporous $CoMoO_4$ nanosheets networks on flexible carbon fabric as a binder-free anode for lithium-ion batteries

Cite this: DOI: 10.1039/x0xx00000x

Received 00th April 2015,
Accepted 00th April 2015

DOI: 10.1039/x0xx00000x

www.rsc.org/

Bo Wang, Songmei Li,* Xiaoyu Wu, Jianhua Liu, Wenming Tian, and Jing Chen

Novel hierarchical $CoMoO_4$ networks assembled by ultrathin mesoporous nanosheets were directly grown on flexible carbon fabric with robust adhesion by a facile hydrothermal method route and a subsequent thermal annealing. The building block nanosheets of the as-prepared $CoMoO_4$ nanoarchitectures shows a mesoporous structure with pores of 2-5 nm, and the thickness as small as 3-5 nm. Based on the time-dependent experiments, a probable growth mechanism of the $CoMoO_4$ nanosheets networks directly grown on the surface of carbon fabric is proposed. Benefitting from the unique structural features, the resultant $CoMoO_4$/carbon fabric electrode exhibits excellent electrochemical performance with a high reversible capacity (1128.05 mAh g^{-1} at a current density of 100 mA g^{-1}) and good cycling stability for highly reversible lithium storage (87.76% retention after 150 cycles). The superior electrochemical performance can be ascribed to the synergistic effect of charge transfer express way, high specific surface area and porous hierarchical structure for electrolyte penetration.

1. Introduction

Owing to environmental pollution issues and the decreasing availability of fossil fuels, the ever-growing demand for sustainable and renewable resources have greatly stimulated the worldwide research on exploiting high-performance renewable and alternative electrical energy storage devices.[1-3] Among emerging energy storage devices, rechargeable lithium ion batteries (LIBs), have drawn intensive research attention and have been widely used in portable electronic devices and electric vehicles in view of their significant advantages of high energy density, long lifespan and environmental benignity.[4-6] To fulfill the requirements of future portable and flexible LIBs, well-designed nanostructures of high-performance, lightweight, flexibility and new attractive electrode materials have been extensively investigated.[7,8]

Transition metal molybdates, $MMoO_4$ (M = Co^{2+}, Ni^{2+}, Zn^{2+}, Mn^{2+} etc) have gradually been considered as promising effective and scalable alternatives to the commercial graphite anode for LIBs in view of their high theoretical capacity, natural abundance, low-cost, and environmental friendliness.[9-12] As an attractive member in the class of the $MMoO_4$ type materials, $CoMoO_4$ have exhibited a higher electrochemical performance than single component oxides due to its multiple oxidation states, higher redox activity and comparative higher electrical conductivity.[13-16] Nevertheless, the large volume changes and stresses occuring during the lithiation and delithiation process commonly cause severe cracking and pulverizing of the electrodes, resulting in a significant capacity fade during cycling and further limiting the commercial applications.[17,18]

Recently, rational design and fabrication of electroactive materials with unique nanostructures grown on conductive substrates to be directly used as free-standing and binder-free electrodes is an effective strategy to improve its electrochemical performance.[19-21] Among various low-dimensional building blocks, mesoporous and thin nanosheets have been regarded as a promising candidate directly grown on the conductive substrates to form an integrated electrode for lithium storage.[22-25] These integrated and binder-free electrodes not only avoid the use of a polymer binder and conductive

Key Laboratory of Aerospace Advanced Materials and Performance of Ministry of Education, School of Materials Science and Engineering, Beihang University, Beijing, 100191, China.

E-mail: songmei_li@buaa.edu.cn; Fax: +86-10-82317103; Tel: +86-10-82317103

Electronic supplementary information (ESI) available. See DOI:

additives in the preparation process of traditional slurry electrode, but also reduce the electron transfer distance and ion diffusion path obviously, and as a result, the reversible capacity especially high rate capacity can be improved.[26,27] In addition, flexible conductive substrates such as commercial Ni foam, carbon cloth, conductive paper, textiles, and polymers films have been widely used as current collectors with soft, bendable and elastic properties to load electroactive materials for fabricating flexible power devices.[28-30] Particularly, carbon fabric (CF), a network of microsized carbon fibers has been reported to be a promising current collector and backbone for directly growing active material since its unique properties including high electrical conductivity, light-weight, chemical stability, superior mechanical flexibility and low cost.[31,32] Therefore, it would be of great significance to develop facile and simple methods to grow mesoporous and ultrathin nanostructures of electroactive materials directly on flexible carbon fabric for high-performance LIBs.

Based on the above considerations, we demonstrate the high-density assembly of ultrathin mesoporous $CoMoO_4$ nanosheets on flexible carbon fabric with a porous network-like structure by a facile and simple hydrothermal approach combined with a post annealing treatment. In view of their apparent advantages, such as high electroactive surface area, ultrathin and porous features, robust mechanical strength, short ion and electron transport path, the $CoMoO_4$/carbon fabric electrode exhibits high specific capacity and excellent cycling stability even under high current densities compared to binder-containing counterparts.

2. Experimental

2.1 Materials and Methods

Growth of network-like $CoMoO_4$ nanosheets on carbon fabric: All chemicals (supplied by Beijing Chemical Co., Ltd.) used were analytical grade and used without further purification. $CoMoO_4$/carbon fabric composites were synthesized by using a simple hydrothermal method followed by a thermal treatment. Prior to deposition, a piece of carbon fabric (CF; ca. 4 cm × 2 cm) was pretreated by rinsed with acetone, deionized water, and absolute ethanol for 15 min, respectively. After drying at 60 ℃ for 5 h, the weight of each treated CF piece was recorded. In a typical process, 0.6 g of $(NH_4)_6Mo_7O_{24}$ $4H_2O$, 3 mmol of $Co(CH_3COO)_2$ $4H_2O$, and 0.72 g of urea were dissolved in 90 mL deionized water to form a transparent pink solution by constant stirring, and then transferred into a 100 mL polytetrafluoroethylene (PTFE) Teflon-lined stainless steel autoclave. Two pieces of treated CF was immersed in the reaction solution and kept at 150 ℃ for 6 h to allow the hydrothermal growth of the CoMo-precursors nanosheets. After that, the autoclave was cooled down to room temperature naturally, and the CF covered with CoMo-precursors nanosheets was removed from the growth solution, rinsed several times with deionized water and absolute ethanol, followed by drying at 60 ℃ for 8 h. Finally, the samples were put in a quartz tube and calcined under the protection of argon gas ambient at 350 ℃ for 3 h at a rate of 2 ℃ min^{-1} to obtain well defined crystallized $CoMoO_4$ nanosheets, and then cooled down to room temperature gradually. In comparison, the $CoMoO_4$ powders were prepared in the same reaction system without the addition of carbon fabric substrates.

2.2 Microscopic Characterization

The crystallographic structures of the samples were determined by a powder X-ray diffraction system (XRD, Rigaku D/max 2200PC) equipped with Cu Kα radiation (λ=0.15418 nm). The morphologies, chemical compositions, and the microstructures of as-prepared products were characterized by field-emission scanning electron microscope (FE-SEM, JEOL JSM-7500F) equipped with an energy dispersive X-ray (EDX) spectrometer, transmission electron microscope (TEM, JEOL JEM-2100F), and X-ray photoelectron spectroscope (XPS, AXIS UTLTRADLD equipped with a dual Mg Ka-Al Ka anode for photoexcitation). The N_2 adsorption-desorption was determined by Brunauer-Emmett-Teller (BET) measurements using an ASAP-2010 surface area analyzer.

2.3 Electrochemical Performance Measurements

The electrochemical performances of the as-prepared products were measured using CR2025-type coin cells assembled in an argon-filled glove box with concentrations of moisture and oxygen below 1.0 ppm. For the coin-cell assembly, the carbon fabric and $CoMoO_4$/carbon fabric composites were punched in the form of 11 mm diameter disks, and then used directly as the working electrode without any conductive additive and polymer binder. Then, we took 10 pieces of samples (carbon fabric and $CoMoO_4$/carbon fabric composites, respectively) and weighed them together. The loading density of the active material ($CoMoO_4$) for the testing electrodes was about 1.2 mg cm^{-2} calculated by the weight of the total mass. A metallic lithium foil served as both the counter electrode and the reference electrode, a polypropylene (PP) microporous film (Celgard 2400) was used as the separator, and a solution of 1 M $LiPF_6$ dissolved in ethylene carbonate/dimethyl carbonate (EC:DMC=1:1 v/v) was used as electrolyte.,

For the comparative study of electrochemical performance, the $CoMoO_4$ powders were also formed into working electrodes. The pasted electrode was prepared by coating an N-methylpyrrolidinone (NMP) slurry composed of 80 wt.% active materials ($CoMoO_4$ powders), 10 wt.% polyvinylidene fluoride (PVDF) and 10 wt.% acetylene black (Super-P) on copper foil current collectors followed by drying at 50 ℃ for 12 h in vacuum.

The galvanostatic charge-discharge and cyclic voltammetry (CV) measurements were carried out on a CT2001A LAND Cell test system (China) and a multichannel Arbin Instruments BT 2000 (USA) unit in the voltage range of 0.005-3.0 V at room temperature (25±1 ℃). Electrochemical impedance spectroscopy (EIS) measurements were performed in the frequency range from 100 kHz to 0.01 Hz on a

PARSTRAT 2273 electrochemical workstation under AC stimulus with a potential amplitude of 5 mV.

3. Results and discussion

The fabrication process of the high-density assembly of ultrathin mesoporous $CoMoO_4$ nanosheets networks on carbon fabric as a binder-free electrode is shown in Scheme 1. The synthesis strategy involves two steps: In the first step, the CoMo-precursor nanosheets were directly grown on the carbon fabric via a facile hydrothermal process. The network-like $CoMoO_4 \cdot xH_2O$ nanoarchitectures are anchored on the skeleton of carbon fabric by spontaneous self-assembly of $CoMoO_4$ nanosheets. After that, the hierarchical $CoMoO_4$ nanosheets network-like structures were converted from the corresponding CoMo-precursor nanosheets architectures subsequently by a thermal treatment under the protection of argon gas ambient at 350 ℃ for 3h.

The crystallinity and phase purity of the as-prepared samples were examined by XRD. Fig. 1a shows the typical XRD patterns of the $CoMoO_4$/carbon fabric composites, together with a bare carbon fabric for comparison. The XRD patterns of carbon fabric display an obvious graphite (002) reflection at 26.21 °.[33] After annealing treatment, the CoMo-precursors/carbon fabric composites can be converted to crystallized $CoMoO_4$/carbon fabric composites and the corresponding XRD pattern can be readily indexed to the monoclinic structured $CoMoO_4$ with a space group of C2/m except for strong peaks originating from the carbon fabric substrate. The diffraction peaks at 26.71 °, 33.59 °, 42.96 ° and 61.52 ° can be indexed as the (002), (222), (113) and (152) crystal planes of monoclinic $CoMoO_4$ (JCPDS card no. 21-0868), as reported previously in the literatures.[20,34] No other peaks that would be associated with other crystalline phases or impurity were observed, indicating the high purity of the obtained products. But for $CoMoO_4$, the amorphous phase attributed to the introduction of ferromagnetism and consequently resulted in a self-assembly of the $CoMoO_4$ nanoparticles.[35,36] In order to eliminate the influence of the carbon fabric substrate, the as-prepared $CoMoO_4$ powders without carbon fabric in the same reaction system were also checked by XRD and the corresponding XRD pattern is shown in Fig. S1 (Supporting Information), where all the peaks can be indexed to monoclinic $CoMoO_4$, which is consistent with the standard XRD pattern of monoclinic $CoMoO_4$ (JCPDS card no. 21-0868).[37,38]

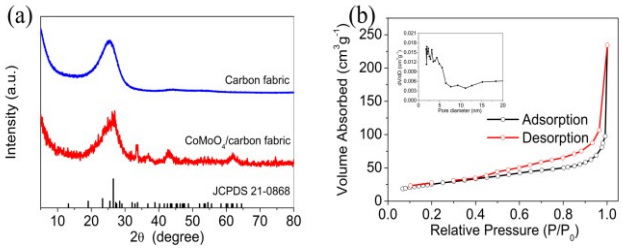

Fig. 1 (a) XRD patterns of carbon fabric, $CoMoO_4$/carbon fabric composites, and the standard XRD pattern of monoclinic $CoMoO_4$. (b) Nitrogen adsorption-desorption isotherms of as-synthesized $CoMoO_4$ nanosheets scratched from the carbon fabric (inset pore size distribution calculated using the BJH method from the desorption curve).

To clearly describe the specific surface area and mesoporous features of $CoMoO_4$ nanoarchitecture, N_2 adsorption-desorption measurements were performed. Fig. 1b depicts the adsorption-desorption isotherm and pore size distribution for the $CoMoO_4$ powder scratched from the carbon fabric. As shown in Fig. 1b, the isotherm can be described as a type IV isotherm curve with a hysteresis loop in the relative pressure (P/P_0) range of 0.5-1.0. This reveals that the as-prepared $CoMoO_4$ nanoarchitecture has a typical mesoporous structure, which is further verified from the Barrett-Joyner-Halenda (BJH) pore size distribution (PSD) curves shown in the inset of Fig. 1b. Nitrogen adsorption-desorption results indicate that the $CoMoO_4$ nanoarchitecture have a specific surface area of 100.26 m^2 g^{-1}. The pore size distribution calculated by desorption isotherm using the Barrett-Joyner-Halenda (BJH) method indicates that the average pore size range of 2-5 nm. Therefore, such unique mesoporous $CoMoO_4$ nanoarchitecture with a high specific surface area have numerous open mesoporous channels, which provided effective active sites for the chemical reactions, high contact area between the electrode and the electrolyte, short pathways for Li^+ diffusion and good accommodation of strain upon cycling.[39]

Fig. 2a shows optical images of the primitive carbon fabric and after annealing treatment by coating with active materials.

Scheme 1. Schematic illustration of the synthetic procedure of $CoMoO_4$/carbon fabric composites.

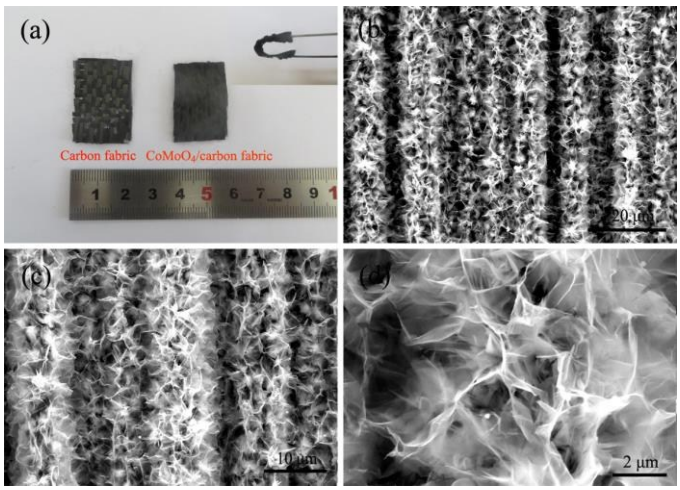

Fig. 2 (a) Photographs of the primitive carbon fabric and $CoMoO_4$/carbon fabric composites (inset the as-synthesized $CoMoO_4$/carbon fabric composites under bending). (b-d) Typical SEM images of $CoMoO_4$/carbon fabric composites at different magnifications.

The obvious color change and the final uniform color of the carbon fabric indicate the uniform coating of active materials. The as-fabricated $CoMoO_4$/carbon fabric composites were light-weight and so great flexibility that it can be folded without any detriment of the structural integrity (as shown in the inset of Fig. 2a). The morphology and microstructure of the bare carbon fabric and as-prepared $CoMoO_4$/carbon fabric composites were evaluated by SEM. A representative low-magnification SEM image (Fig. S2 Supporting Information) of the individual carbon fiber in the as-received carbon fabric before the $CoMoO_4$ nanosheet growth with a smooth surface and a diameter of about 7 μm. Fig. 2b-d show the SEM images of the $CoMoO_4$/carbon fabric composites at different magnifications. As shown in Fig. 2b, the whole surface of carbon fabric is uniformly covered by high density of well-defined network-like structues that are composed by numerous interconnected nanosheets with each other. resulting them to become thicker and with a rougher surface. From the higher-magnification SEM images (Fig. 2c-d), it can be seen clearly that the $CoMoO_4$ nanosheets are interconnected with each other to form a hierarchical network structue, which creates loose porous nanostructures with abundant open space and electroactive surface sites. The lateral size of individual nanosheets was about serveral micrometers, while the thickness of nanosheets is less than 5 nm. Meawhile, the morphologies of bending, curling, and crumpling are due to the much larger lateral size than the thickness. Interestingly, the void space between neighboring nanosheets is still sufficient, which is favorable for easy electrolyte penetration and accommodation of volume expansion during lithiation/delithiation process. Fig. 3a-e displays the elemental mapping images of $CoMoO_4$/carbon fabric composites, which indicate that the cobalt, molybdenum, oxygen, and carbon elements were dispersed uniformly and continuously. Furthermore, the energy dispersive EDS analysis of the as-prepared $CoMoO_4$/carbon fabric composites, shown in Fig. 3f, demonstrates the presence of Co, Mo, O and C elements, arising from the carbon fabric substrate.

The detailed morphologies and microstructures of the $CoMoO_4$ architectures were further investigated by TEM (Fig.

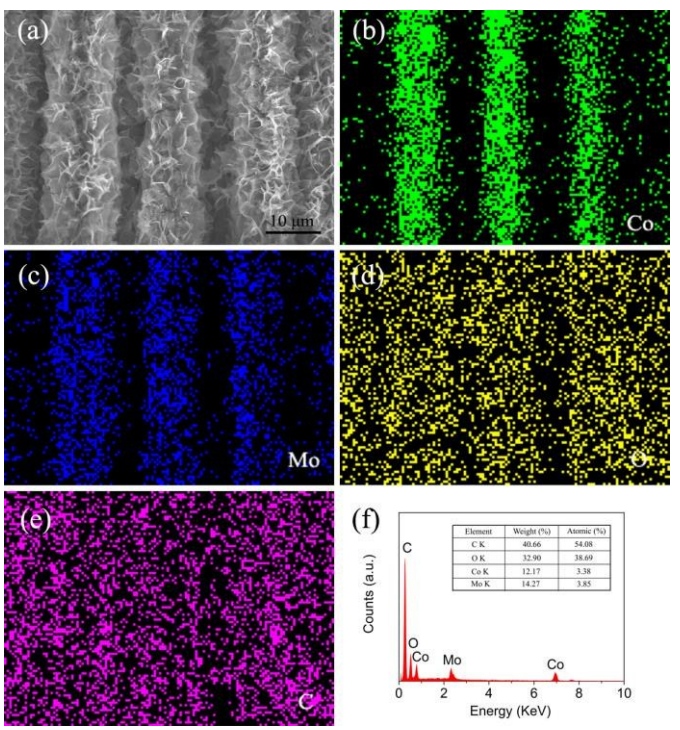

Fig. 3 (a) SEM image of $CoMoO_4$/carbon fabric composites; EDS elemental mappings of (b) cobalt, (c) molybdenum, (d) oxygen, and (e) carbon, respectively. (f) EDS spectrum of $CoMoO_4$/carbon fabric composites.

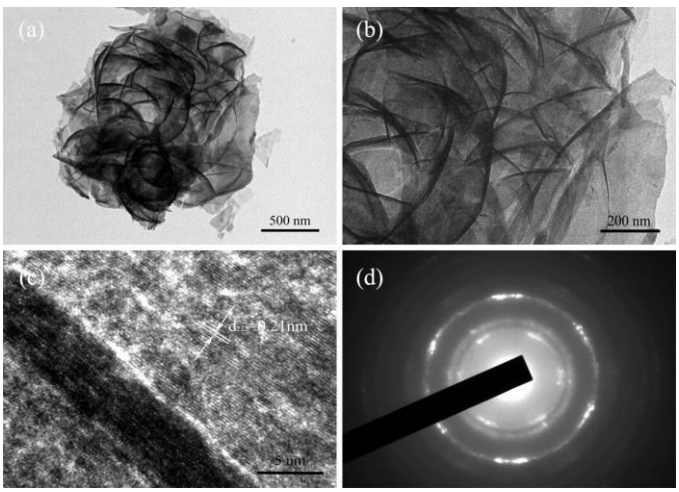

Fig. 4 (a, b) TEM images, (c) HRTEM image and (d) SAED pattern of network-strucutred $CoMoO_4$ nanosheets scratched from the carbon fabric.

4). As shown in Fig. 4a, the TEM images also confirm the interconnected and network-like porous structure of the products built up of ultrathin nanosheets, which are in good agreement with the results of SEM images. As seen from the higher magnified TEM image (Fig. 4b), the average thickness of an individuate nanosheet is about 3-5 nm. A representative high-resolution TEM (HRTEM) image is shown in Fig. 4c, where a distinct set of visible lattice fringes with an inter-planar spacing of 0.21 nm can be clearly observed, corresponding to the (222) plane of $CoMoO_4$.[34] Interestingly, as depicted in the higher magnification TEM image of an individuate nanosheet (Fig. S3 Supporting Information), numerous mesopores are uniformly distributed throughout the whole surface of nanosheets, which were generated by the rapid release of water molecules during the conversion of CoMo-precursors into $CoMoO_4$ crystals. The size of the interparticle mesopores in the nanosheets is estimated to be in the range of 2-5 nm. The ultrathin and mesoporous characteristics of the nanosheets give rise to large specific surface urea, leading to more efficient utilization of the active material, which is also beneficial to lithium-ion transport and accommodate volume variation of the active materials during charging/discharging.[40] In addition, the corresponding selected area electron diffraction (SAED) pattern (Fig. 4d) indicates the polycrystalline nature of the $CoMoO_4$ nanosheets, which is consistent with the XRD characterization.

The elemental composition and the surface chemical bonding state of as-prepared $CoMoO_4$/carbon fabric composites was evaluated by XPS measurements, and the corresponding results are presented in Fig. 5. Fig. 5a displays the survey XPS spectrum of the materials, which mainly contain C 1s, Co 2p, Mo 3d and O 1s core level peaks confirm the presence of Ni, Mo, C and O elements in $CoMoO_4$/carbon fabric composites. The Mo 3d and Co 2p high-resolution spectra were fitted by using a Gaussian fitting method. As shown in Fig. 5b and c, a of Mo 3d, respectively. The binding energy and the splitting doublet of Mo $3d_{3/2}$ and Mo $3d_{5/2}$ peaks with binding energy values of 233.2 eV and 236.3 eV can be observed in the region width (△Mo 3d = 3.1 eV) are characteristics of Mo^{6+} oxidation state in $CoMoO_4$/carbon fabric composites.[41,42] The Co 2p core level spectrum shows two speaks with binding energies of 781 and 797 eV, which can be assigned to Co $2p_{3/2}$ and Co $2p_{1/2}$, representing the existence of the Co^{2+}.[34] Fig. 4d represents the C 1s core level spectrum of the $CoMoO_4$/carbon fabric composites. The binding energy peak at 284.7 eV corresponds to sp^2 hybridized carbon.[43] Fig. S4 (Supporting Information) shows the high-resolution spectrum of the O 1s region; the binding energy (O 1s) is 532 eV which corresponds to lattice oxygen.[44] The XPS results confirm that the valence of Co, Mo and O elements are +2, +6 and -2, respectively.

To explore the formation mechanism of the hierarchical $CoMoO_4$ nanosheets nanoworks grown on the surface of carbon fabric, a series of time-dependent experiments with different hydrothermal reaction times were performed. Fig. 6 shows SEM images of the morphological evolution of the products obtained along with the elongation of reaction time (0.5, 2, 4, and 6 h). Before the reaction, there were no nanosheets on the surface of the carbon fabric as shown in Fig. S2 (Supporting Information). It was found that some small $CoMoO_4$ clusters appeared on the surface of carbon fabric after the hydrothermal reaction for 0.5 h (Fig. 6a). With prolonging the reaction time to 2 h, the loose and well-distributed $CoMoO_4$ clusters were formed on the surface of carbon fabric (Fig. 6b). Impressively, when the reaction time was further prolonged to 4 h, the interconnected $CoMoO_4$ nanosheets have been completely coated on the surface of the carbon fabric by replacing the clusters (Fig. 6c). As the reaction time increased, the carbon fabric surface was covered by more nanosheets to form a network-like structure and spread uniformly on the substrate after 6 h (as shown in the Fig. 6d). Meanwhile, these small nanosheets grow up to form a larger size with greater thickness,

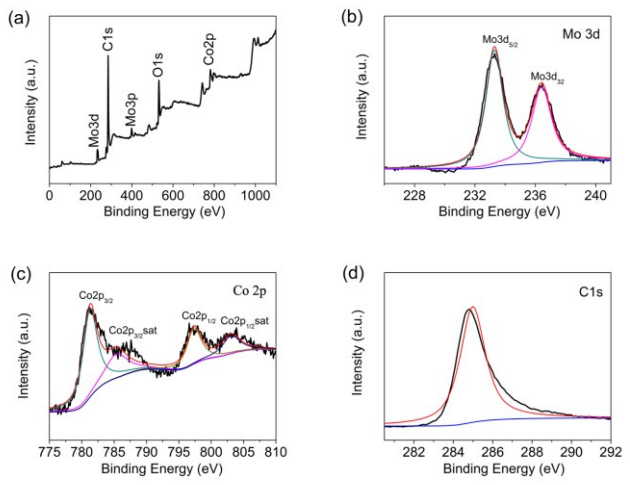

Fig. 5 The XPS spectra (a) The survey XPS spectrum and high-resolution XPS spectra of (b) Mo 3d, (c) Co 2p and (d) C 1s for the $CoMoO_4$/carbon fabric composites.

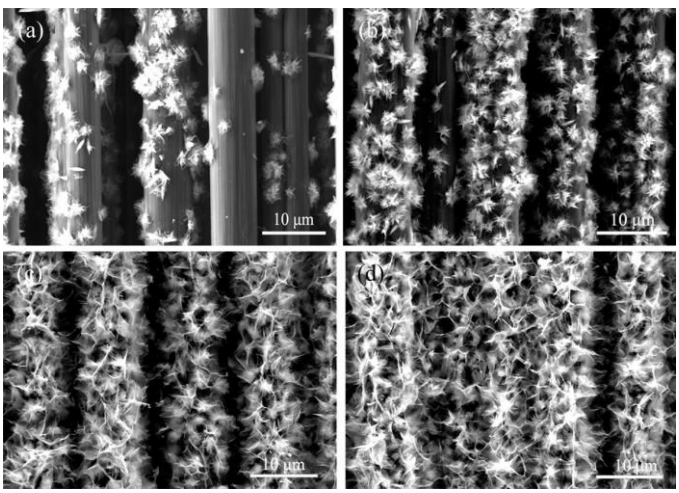

Fig. 6 SEM images of $CoMoO_4$/carbon fabric composites obtained at different hydrothermal growth times: (a) 0.5 h, (b) 2 h, (c) 4 h, and (d) 6 h.

leading to more void spaces between the each nanosheets. These results suggest that it is possible to control the architecture of $CoMoO_4$ by controlling the hydrothermal reaction time. The XRD patterns (Fig. S5 Supporting Information) show that all products obtained at 0.5, 2, 4 and 6 h reaction time can be indexed to a monoclinic $CoMoO_4$. With the time increasing, the products crystalize much better and obvious diffraction peaks appear.

Based on the above experimental observations, a schematic illustration of the speculative growth mechanism of the network-like $CoMoO_4$ nanosheets on the surface of carbon fabric is proposed and shown in Scheme 2. At the early stage of reaction, many nanoparticles appeared and grew at the surface of carbon fabric. This was the nucleation stage, with numerous $CoMoO_4$ precursor ($CoMoO_4 \cdot xH_2O$) nucleation centers derived from the combination of Co^{2+} and MoO_4^{2-} ions. As the reaction proceeded, the crystal growth stage transferred to a kinetically controlled process. The derived nucleation centers grew to small $CoMoO_4$ precursor nanosheets and gradually grew into larger nanosheets. Finally, the numerous nanosheets assembled into network-like porous architectures were uniformly and densely distributed on the substrate according to the Ostwald ripening mechanism.

Motivated by the interesting 3D hierarchical architectures composed of carbon cloth with high conductivity and interconnected ultrathin mesoporous $CoMoO_4$ nanosheets with void spaces, we have evaluated the electrochemical lithium storage properties of $CoMoO_4$/carbon fabric composites for their potential applications as additive-free integrated electrodes in LIBs. Fig. 7a displays representative CV curves of $CoMoO_4$/carbon fabric electrode for the initial five cycles at a scan rate of 0.1 mV s^{-1} in the voltage window of 0.005-3.0 V vs. Li^+/Li. The first CV curve is obviously different from the following cycles and the following CV curves are almost overlapped from the second to the third cycle, presenting excellent reversible performances except for the irreversible reactivity in the first cycle. In the first cycle, there are an obvious reduction peak around 0.26 and a poorly defined anodic peak at 1.62V, which is attributed to the electrochemical reduction reaction of $CoMoO_4$ to metallic Co and Mo, lithium ion insertion into carbon fabric and formation of solid-electrolyte interface (SEI) due to the reduction of solvents in the electrolyte.[18, 45-47] In the anodic scan, two poorly defined

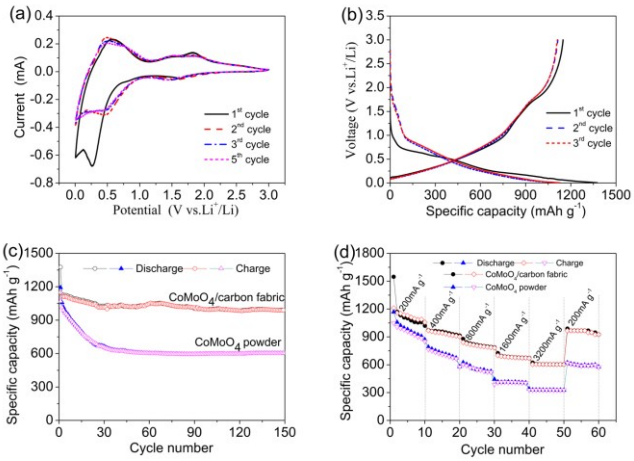

Fig. 7 (a) Cyclic voltammograms of the $CoMoO_4$/carbon fabric electrode for the initial five cycles at a scan rate of 0.1 mV s^{-1} in the voltage range of 0.005-3.0 V, (b) Galvanostatic charge-discharge voltage profiles of $CoMoO_4$/carbon fabric electrode for the first three cycles at a current density of 100 mA g^{-1}, (c) Comparison of cycling performance of the $CoMoO_4$/carbon fabric electrode with $CoMoO_4$ powder pasted electrode, (d) Comparison of rate performance of the $CoMoO_4$/carbon fabric electrode with $CoMoO_4$ powder pasted electrode.

anodic peaks are observed at 1.53 V and 1.82 V, corresponding to the oxidation of Co and Mo to form CoO and MoO_3,[48,49] while the peak around 0.56 V is ascribed to lithium ion extraction from carbon fabric and the co-efficiency between the carbon fabric and the electrode material.[50,51] Remarkably, from the second cycle onwards, the reduction peak located at 0.26V in the first cycle is moved to 0.49 V and the CV curves overlap very well, indicating good reversibility of the electrochemical reactions. The slight shift of the reduction peak to higher potential in the following cycles might be related to some activation process caused by the Li^+ insertion in the first cycle, indicating the slightly easier reduction in the subsequent cycles. Based on the above CV analysis and previous reported lithium storage mechanisms of $CoMoO_4$, the complete electrochemical reactions in the as-prepared $CoMoO_4$/carbon fabric composite might be expressed as follows: [13,17]

$$CoMoO_4 + 8Li^+ + 8e^- \rightarrow Co + Mo + 4Li_2O \quad (1)$$

$$Co + Li_2O \rightarrow CoO + 2Li^+ + 2e^- \quad (2)$$

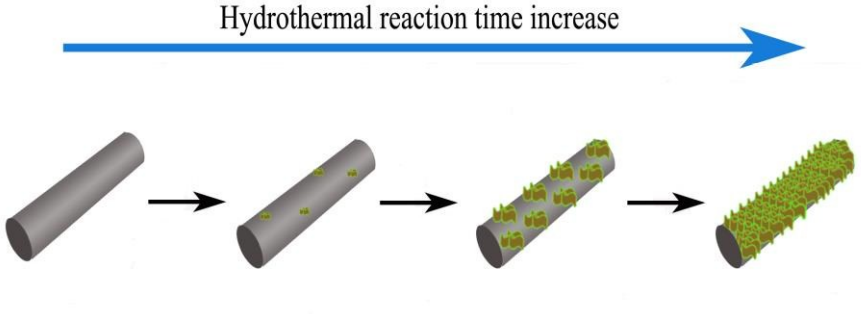

Scheme 2. Schematic illustration of growth process of the network-like $CoMoO_4$ architectures on the surface of carbon fabric.

$$Mo + 3Li_2O \rightarrow MoO_3 + 6Li^+ + 6e^- \quad (3)$$

$$Co + Mo + 4Li_2O \leftrightarrow CoO + MoO_3 + 8Li^+ + 8e^- \quad (4)$$

To evaluate the electrochemical performance of the $CoMoO_4$/carbon fabric electrode, typical voltage-specific capacity curves were recorded at a current density of 100 mA g^{-1} in the voltage range of 0.005-3.0 V vs. Li^+/Li. As shown in Fig. 7b, the charge-discharge voltage profiles of the $CoMoO_4$/carbon fabric electrode show a more vertical line in low frequency region compared to the $CoMoO_4$ powder pasted electrode, indicating fabric electrode delivers the initial discharge and charge capacities of 1376.47 and 1148.81 mAh g^{-1}, respectively, corresponding to a moderate columbic efficiency of 83.46%. The irreversible capacity loss during the first cycle can be commonly attributed to the incomplete restoration of metallic Co and Mo into the original oxides and irreversible lithium loss due to the formation of a solid-electrolyte interface layer, which is similar to other reported results.[33,47] Nevertheless, the voltage profiles are approximately overlapping except for the initial discharge, indicating excellent stability of the hybrid structure for reversible lithium storage. The columbic efficiency increases rapidly to 98.7% in the second cycle and then remains above 98% in the subsequent cycles. The overlapping of the following discharge-charge curves reveals good stability and reversibility of the conversion reactions.

The cycling stability of the $CoMoO_4$/carbon fabric and $CoMoO_4$ powder pasted electrodes were investigated for comparison, as shown in Fig. 7c. From the second cycle onwards, the discharge capacity of the $CoMoO_4$/carbon fabric electrode only decreases slightly. After 150 cycles at 100 mA g^{-1}, a reversible discharge capacity as high as 990.02 mAh g^{-1} is retained, corresponding to 87.76% of the discharge capacity in the second cycle. Apparently, these results are in stark contrast to those of $CoMoO_4$ powder pasted electrode, which show continuous and progressive capacity fading along with the cycling under the same testing conditions. After 150 cycles, the discharge capacity only remained at 602.83 mAh g^{-1} (57% of discharge capacity in the second cycle). These results demonstrate that the $CoMoO_4$/carbon fabric electrode exhibits significantly improved cycling stability compared to $CoMoO_4$ powder pasted electrode. In order to get rid of the influence of the carbon fabric, the pure carbon fabric based electrode was also analysed, exhibiting a low capacity (Fig. S6, Supporting Information). When coated with the electrode material, the carbon fabric has relatively little contact with the electrolyte. Therefore, the substrate contributes little to the whole capacity, while its high conductivity plays an important role in the good stability of the anodes.

An additional advantage of the $CoMoO_4$/carbon fabric electrode is the enhancement of the rate capability. To further evaluate the rate capability, the electrodes were cycled at various current densities ranging from 200 to 3200 mA g^{-1}, and finally returned to 200 mA g^{-1}. As shown in Fig. 7d, the specific capacity of the $CoMoO_4$/carbon fabric electrode decreases steadily as the current density increases, but still retains high values. It is worth noting that even cycled at a high current density of 3200 mA g^{-1}, a stable reversible capacity of about 604 mAh g^{-1} is still retained. To demonstrate the great advantage of this hierarchical $CoMoO_4$/carbon fabric electrode for LIBs, the rate capability of $CoMoO_4$ powder pasted electrode was also investigated under the same conditions. Remarkably, these values are much higher than those of the $CoMoO_4$ powder pasted electrode ($\sim$326 mAh g^{-1}). More importantly, the specific capacity of the electrode can be nearly recovered to its initial reversible values when the current density is returned back to 200 mA g^{-1}, which indicates the excellent rate capability of the ultrathin mesoporous $CoMoO_4$ nanosheets architectures on the carbon fabric. Compared to the $CoMoO_4$/carbon fabric electrode, the $CoMoO_4$ powder pasted electrode shows a much poor rate performance as a result of sluggish ionic adsorption/diffusion kinetics and poor electronic conductivity.

To further gain insight into the superior rate capability and cyclability of $CoMoO_4$/carbon fabric electrode, the as-fabricated $CoMoO_4$ powder pasted and $CoMoO_4$/carbon fabric electrodes at open-circuit potential were analyzed by EIS. As shown in Fig. 8a, the Nyquist plots are composed of a semicircle in the high-middle frequency region and a slope line in the low frequency region. Obviously, the diameter of the semicircle for $CoMoO_4$/carbon fabric electrode in the high-

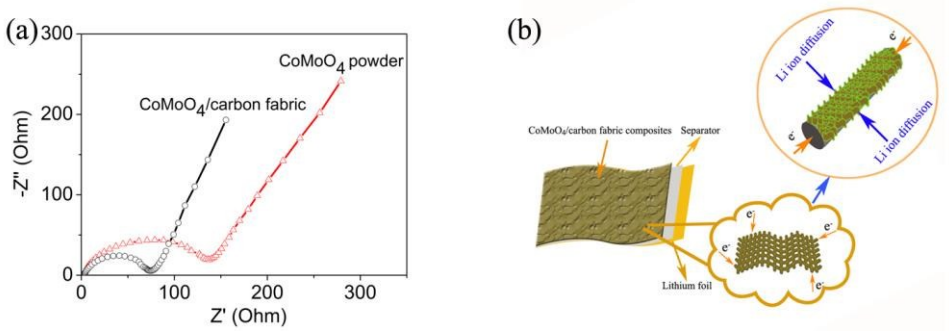

Fig.8 (a) Nyquist plots of the $CoMoO_4$/carbon fabric and $CoMoO_4$ powder pasted electrodes measured with an amplitude of 5 mV over the frequency range of 100 kHz and 0.01Hz. (b) Schematic illustration of $CoMoO_4$/carbon fabric composites as electrode materials for LIBs.

middle frequency region is much smaller than that of the $CoMoO_4$ powder pasted electrode, which indicates that $CoMoO_4$/carbon fabric electrode possess the lowest contact and electron-transfer resistances, indicating that the introduction of carbon fabric and the interfacial interaction between $CoMoO_4$ nanosheets and carbon fabric largely improves the conductivity of $CoMoO_4$/carbon fabric electrode. The slope of a straight line in the low frequency region can reflect the diffusive resistance resulting from the diffusion of active species in the electrolyte.[52,53] As shown in Fig. 8a, the $CoMoO_4$/carbon fabric electrode show a more vertical line in low frequency region compared to the $CoMoO_4$ powder pasted electrode, indicating the small diffusive resistance of the electroactive species in the electrolyte. This can be attributed to the unique ultrathin and mesoporous features of $CoMoO_4$ nanosheets and porous network-like structure of $CoMoO_4$/carbon fabric composites. Therefore, the above results indicate the perfect ion diffusion and charge transmission in the $CoMoO_4$/carbon fabric electrode.

Based on the results mentioned above, the excellent electrochemical performance of the $CoMoO_4$/carbon fabric electrode can be attributed to the rationally designed nanostructure and outstanding structural features of each component. Firstly, the presence of carbon fabric substrate with relatively good electrical conductivity and flexible nature, which can serves as the superb highways for fast electron transportation and buffering matrix to counteract the pulverization problem. Moreover, the ultrathin and mesoporous features of the $CoMoO_4$ nanosheets and void spaces between the neighboring nanosheets provide a shorter pathway for Li-ion diffusion, more reactive sites for Li-ion intercalation, and make the electrolyte contact efficiently with the electroactive material, thus, enhancing the reversibility of the anode significantly (As shown in Fig. 8b). Furthermore, the hierarchical $CoMoO_4$ nanosheets are directly grown on the conductive carbon fabric with robust adhesion to form an integrated electrode, which provides more importantly good electrical contact with the conductive substrate, and enhance the charge rate of the electrode for high-powder applications. As a result, the flexible $CoMoO_4$/carbon fabric electrode exhibits high specific capacity, good cycling stability, and outstanding rate performance, thereby offering a very promising potential for applications in flexible batteries.

4. Conclusions

In summary, interconnected $CoMoO_4$ network-like architectures assembled with ultrathin nanosheets directly grown on carbon fabric substrates were successfully fabricated by a facile hydrothermal method combined with a post annealing treatment. The carbon fabric substrate with relatively good electrical conductivity facilitated fast electron transportation and the ultrathin mesoporous $CoMoO_4$ nanosheets networks shortens the ion diffusion paths and ensured high utilization of the electroactive material. The resultant binder-free $CoMoO_4$/carbon fabric electrode exhibits excellent electrochemical performance with a higher reversible capacity of 1128.05 mAh g^{-1} at a current density of 100 mA g^{-1} and much better cycling stability for highly reversible lithium storage (87.76% retention after 150 cycles) compared to binder-containing counterparts. In view of the excellent electrochemical performance and the facile and cost-effective synthesis, the flexible $CoMoO_4$/carbon fabric composites might hold great promise as advanced electrode materials for flexible high-performance lithium ion batteries.

Acknowledgements

This work was financially supported by the National Natural Science Foundation of China (Grant No. 51271012) and Innovation Foundation of Beihang University for PhD Graduates. The authors thank the Analysis and Testing Center of the School of Materials Science and Engineering of Beihang University for support.

Notes and references

1 J. Tollefson, *Nature*, 2008, **456,** 436-440.
2 J. B. Goodenough, and K. S. Park, *J. Am. Chem. Soc.*, 2013, **135,** 1167.
3 P. G. Bruce, B. Scrosati, and J -M. Tarascon, *Angew. Chem. Int. Ed.*, 2008, **47,** 2930.
4 H. B. Wu, J. S. Chen, H. H. Hng, and X. W. Lou, *Nanoscale*, 2012, **4,** 2526.
5 J. Jiang, Y. Li, J. Liu, X. Huang, C. Yuan, and X. W. Lou, *Adv. Mater.*, 2012, **24,** 5166.
6 X. -L. Huang, R. -Z. Wang, D. Xu, Z. -L. Wang, H. -G. Wang, J. -J. Xu, Z. Wu, Q. -C. Liu, Y. Zhang, and X. -B, Zhang, *Adv. Funct. Mater.*, 2013, **23,** 4274.
7 X. Wang, X. Lu, B. Liu, D. Chen, Y. Tong, and G. Shen, *Adv. Mater.*, 2014, **26,** 4763.
8 L. Li, Z. Wu, S. Yuan and X. Zhang, *Energy Environ. Sci.*, 2014, **7,** 2101.
9 Y. Ding, Y. Wan, Y. -L. Min, W. Zhang, and S. -H. Yu, *Inorg. Chem.*, 2008, **47,** 7813.
10 T. Yang, H. Zhang, Y. luo, L. Mei, D. Guo, Q. Li, and T. Wang, *Electrochim. Acta*, 2015, **158,** 327.
11 J. Haetge, I. Djerdj, and T. Brezesinski, *Chem. Commun.*, 2012, **48,** 6726.
12 K. -S. Park, S. -D. Seo, H. -W. Shim, and D. -W. Kim, *Nanoscale Res. Lett.*, 2012, **7,** 35.
13 L. R. Hou, H. Hua, S. J. Liu, G. Pang, and C. Z. Yuan, *New J. Chem.*, 2015, **39,** 5507.
14 X. Yu, B. Lu, and Z. Xu, *Adv. Mater.*, 2014, **26,** 1044.
15 L. -Q. Mai, F. Yang, Y. -L. Zhao, X. Xu, L. Xu, and Y. Z. Luo, Nat.Commun., 2011, **2,** 381.
16 H. Yu, C. Guan, X. Rui, B. Ouyang, B. Yadian, Y. Huang, H. Zhang, H. E. Hoster, H. J. Fan, and Q. Yan, *Nanoscale*, 2014, **6,** 10556.
17 X. -J. Ma, L. -B. Kong, W. -B. Zhang, M. -C. Liu, Y. -C. Luo, and L. Kang, *RSC Adv.*, 2014, **4,** 17884.

18 N. N. Leyzerovich, K. G. Bramnik, T. Buhrmester, H. Ehrenberg, and H. Fuess, *J. Power Sources*, 2004, **127,** 76.
19 G. Zhang and X. W. Lou, *Adv. Mater.*, 2013, **25,** 976.
20 D. Guo, H. Zhang, X. Yu, M. Zhang, P. Zhang, Q. Li, and T. Wang, *J. Mater. Chem. A*, 2013, **1,** 7247.
21 X. -L. Huang, X. Zhao, Z. -L. Wang, L. -M. Wang, and X.-B. Zhang, *J. Mater. Chem.*, 2012, **22,** 3764.
22 X. Fan, Y. Shi, L. Gou, and D. Li, *Electrochim. Acta*, 2014, **142,** 268.
23 X. Wang, Y. Fan, R. A. Susantyoko, Q. Xiao, L. Sun, D. He, and Q. Zhang, *Nano Energy*, 2014, **5,** 91.
24 A. K. Mondal, D. Su, S. Chen, K. Kretschmer, X. Xie, H. Ahn, and G. Wang, *ChemPhysChem*, 2015, **16,** 169.
25 Y. Huang, X. -L. Huang, J. -S. Lian, D. Xu, L. -M. Wang and X. -B. Zhang, *J. Mater. Chem.*, 2012, **22,** 2844.
26 G. Gao, H. B. Wu, and X. W. Lou, *Adv. Energy Mater.*, 2014, **4,** 1400422.
27 X. Zhao, B. Liu, C. Hu, and M. Cao, *Chem. Eur. J.*, 2014, **20,** 467.
28 Q. Wang, X. Wang, B. Liu, G. Yu, X. Hou, D. Chen, and G. Shen, *J. Mater. Chem. A*, 2013, **1,** 2468.
29 G. Zhou, F. Li and H. -M. Cheng, *Energy Environ. Sci.*, 2014, **7,** 1307.
30 H. Yu, C. Zhu, K. Zhang, Y. Chen, C. Li, P. Gao, P. Yang and Q. Ouyang, *J. Mater. Chem. A*, 2014, **2,** 4551.
31 J. Du, G. Zhou, H. Zhang, C. Cheng, J. Ma, W. Wei, L. Chen, and T. Wang, *ACS Appl. Mater. Interfaces*, 2013, **5,** 7405.
32 M. -S. Balogun, M. Yu, C. Li, T. Zhai, Y. Liu, X. Lu, and Y. Tong, *J. Mater. Chem. A*, 2014, **2,** 10825.
33 L. F. Shen, Q. Che, H. S. Li, and X. G. Zhang, *Adv. Funct. Mater.*, 2014, **24,** 2630.
34 D. Cai, B. Liu, D. Wang, L. Wang, Y. Liu, H. Li, Y. Wang, Q. Li and T. Wang, *J. Mater. Chem. A*, 2014, **2,** 4954.
35 B. B. Straumal, S. G. Protasova, A. A. Mazilkin, B. Baretzky, A. A. Myatiev, P.B. Straumal, T. Tietze, G. Schutz, and E. Goering, *Mater. Lett.*, 2012, **71,** 21.
36 M. -C. Liu, L. -B. Kong, C. Lu, X. -M. Li, Y. -C. Luo, and L. Kang, *Mater. Lett.*, 2013, **94,** 197.
37 G. K. Veerasubramani, K. Krishnamoorthy, S. Radhakrishnan, N. Kim, and S. J. Kim, *Int. J. Hydrogen Energy.*, 2014, **39,** 5186.
38 M. -C. Liu, L. -B. Kong, C. Lu, X. -J. Ma, X. -M. Li, Y. -C. Luo, and L. Kang, *J. Mater. Chem. A*, 2013, **1,** 1380.
39 S. E. Moosavifard, J. Shamsi, S. Fani, and S. Kadkhodazade, *RSC Adv.*, 2014, **4,** 52555.
40 W. Hong, J. Wang, P. Gong, J. Sun, L. Niu, Z. Yang, Z. Wang, and S. Yang, *J. Power Sources*, 2014, **270,** 516.
41 X. W. Xu, J. F. Shen, N. Li, and M. X. Ye, J. Alloys Comp., 2014, **616,** 58.
42 Q. Zhang, Y. Deng, Z. Hu, Y. Liu, M. Yao, and P. Liu, *Phys. Chem. Chem. Phys.*, 2014, **16,** 23451.
43 K. Xu, J. Chao, W. Li, Q. Liu, Z. Wang, X. Liu, R. Zou, and J. Hu, *RSC Adv.*, 2014, **4,** 34307.
44 X. Y. Wu, J. Du, H. B. Li, M. F. Zhang, B. J. Xi, H. Fan, Y. C. Zhu, and Y. T. Qian, *J. Solid State Chem.*, 2007, **180,** 3288.
45 L. N. Gao, X. F. Wang, Z. Xie, W. F. Song, L. J. Wang, X. Wu, F. Y. Qu, D. Chen and G. Z. Shen, *J. Mater. Chem. A*, 2013, **1,** 7167.
46 B. Wang, S. M. Li, J. H. Liu, M. Yu, B. Li, and X. Y. Wu, *Electrochim. Acta*, 2014, **146,** 679.
47 W. L. Yao, J. Yang, J. L. Wang, and L. Tao, *Electrochim. Acta*, 2008, **53,** 7326.
48 L. Zhou, D. Zhao, and X. W. Lou, *Adv. Mater.*, 2012, **24,** 745.
49 P. Meduri, E. Clark, J. H. Kim, E. Dayalan, G. U. Sumanasekera, M. K. Sunkara, *Nano Lett.*, 2012, **12,** 1784.
50 X. J. Hou, X .F. Wang, B. Liu, Q. F. Wang, T. Luo, D. Chen, and G. Z. Shen, *Nanoscale*, 2014, **6,** 8858.
51 J. K. Ryu, S. -W. Kim, K. Kang, and C. B. Park, *ACS Nano*, 2010, **4,** 159.
52 M. Li, S. Xu, T. Liu, F. Wang, P. Yang, L. Wang, and P. Chu, *J. Mater. Chem. A*, 2013, **1,** 532.
53 S. M, Li, B. Wang, J. H. Liu, and M. Yu, *Electrochim. Acta*, 2014, **129,** 33.

The table of contents:

Self-assembly of ultrathin mesoporous $CoMoO_4$ nanosheets networks on flexible carbon fabric as a binder-free anode for lithium-ion batteries

Bo Wang, Songmei Li*, Xiaoyu Wu, Jianhua Liu, Wenming Tian, and Jing Chen

Key Laboratory of Aerospace Advanced Materials and Performance of Ministry of Education, School of Materials Science and Engineering, Beihang University, Beijing 100191, P. R. China

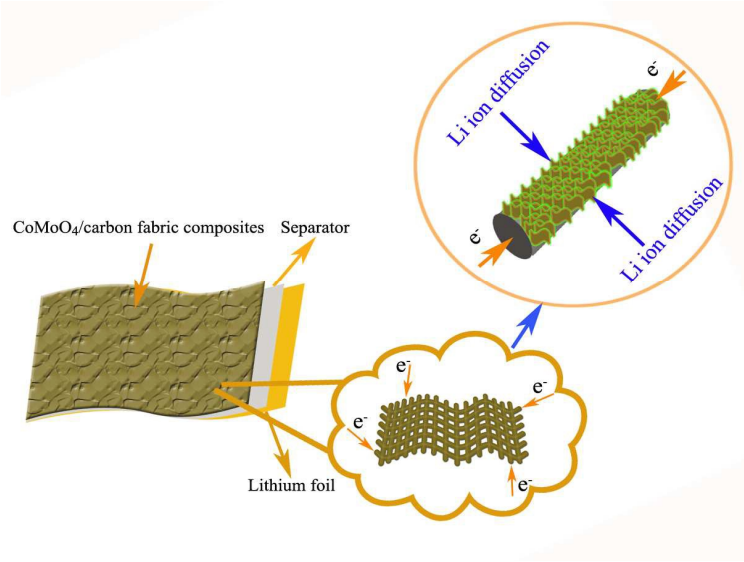

Novel hierarchical $CoMoO_4$ networks assembled by ultrathin mesoporous nanosheets are directly grown on flexible carbon fabric as integrated anodes for highly efficient and reversible lithium storage.